Weather and Climate Extremes 51 (2026) 100873

Contents lists available at ScienceDirect

Weather and Climate Extremes

journal homepage: www.elsevier.com/locate/wace

Evaporative demand drought index for monitoring and analyzing drought conditions in arid regions of Asia and Africa

Akinwale T. Ogunrinde [a,*], Paul Adigun [b], Xian Xue [a], Dairaku Koji [b], Ermias S. Brhane [b]

[a] Key Laboratory of Ecological Safety and Sustainable Development in Arid Lands, Northwest Institute of Eco-Environment and Resources, Chinese Academy of Sciences, Lanzhou, Gansu, China
[b] Department of Engineering Mechanics and Energy, University of Tsukuba, 3F300 Tennodai 1-1-1, Tsukuba, 305-8573, Japan

ARTICLE INFO

Keywords:
Flash drought
Evaporative demand
Arid climates
Drought indices
Climate change

ABSTRACT

In arid regions of Asia and Africa, where evaporative demand exerts increasing control over drought dynamics under climate change, this study introduces the Evaporative Demand Drought Index (EDDI) as a complementary tool to precipitation-based indices for improved monitoring of flash droughts and evapotranspiration-driven moisture stress. Using ERA5-Land reanalysis data at 0.1° resolution, EDDI was calculated using the Penman-Monteith formulation across timescales from sub-weekly to 12 months period. Its performance was evaluated against the Standardized Precipitation Index (SPI) and Standardized Precipitation-Evapotranspiration Index (SPEI) through modified Mann-Kendall trend analysis, Sen's slope estimation, Spearman rank correlations, run theory-based drought characterization, and a detailed examination of the 2010 drought event. EDDI showed strong inverse correlations with SPI and SPEI (ranging from −0.41 to −0.91), with the strongest association, −0.91, observed between EDDI and SPEI at the 1-month scale in the Sahara (SAH) region. Across the studied arid domains, EDDI revealed more pronounced drying trends than those identified by SPI or SPEI, attributable to significant increases in temperature (0.02–0.05 °C year^{-1}) and reference evapotranspiration (ET_o) (2.0–5.16 mm year^{-1}). Drought frequency intensified in most regions after 2000, except on the Tibetan Plateau (TIB). During the 2010 drought episode, EDDI detected the onset of the drought weeks earlier than SPI, demonstrating its sensitivity to rapid increases in evaporative demand. These findings indicate that EDDI serves as a valuable complementary index, capturing aspects of drought related to atmospheric evaporative demand and rapid-onset events that may be underrepresented by precipitation-focused metrics. Integrating EDDI into operational drought early warning systems for arid regions could enhance monitoring capabilities and support more informed decision-making for drought risk management under ongoing climate change.

1. Introduction

Drought is typically defined as a temporary deviation from long-term climatological water availability, resulting from sustained precipitation deficits, increased atmospheric evaporative demand, or their combined effects. It is a reoccuring hydroclimatic hazard with far-reaching impacts on ecosystems and socioeconomic systems, particularly agricultural productivity, food supply, and water security (Ng et al., 2024; Kapoor et al., 2020). Asia has experienced frequent and severe drought events that affect large populations, with substantial impacts on agriculture and water resources. Disaster inventories and regional assessments consistently rank drought among the most damaging climate hazards, although cumulative economic losses remain uncertain due to reporting limitations (Guha-Sapir et al., 2021; UNCCD, 2022). In Africa, prolonged droughts have driven widespread crop failures, persistent water scarcity, and heightened food insecurity, especially in North Africa and the Sahel, where livelihoods largely depend on rain-fed agriculture (Tanarhte et al., 2024). Climate change is expected to amplify drought risk globally. According to the Intergovernmental Panel on Climate Change, continued warming will increase demand for atmospheric moisture and alter precipitation regimes, increasing the likelihood of drought in many regions (IPCC, 2021). These processes are projected to further stress water resources, reduce agricultural yields, and increase socioeconomic vulnerability across Asia and Africa, underscoring the need for improved drought monitoring and assessment to support effective adaptation and risk management.

* Corresponding author.
E-mail address: ogunrindeakinwale@nieer.ac.cn (A.T. Ogunrinde).

https://doi.org/10.1016/j.wace.2026.100873
Received 1 August 2025; Received in revised form 18 December 2025; Accepted 17 February 2026
Available online 18 February 2026

Drought monitoring commonly relies on standardized indices that summarize hydroclimatic anomalies into quantitative measures suitable for operational use and decision-making (Safdar et al., 2023). These indices differ in their input variables, assumptions, and the components of the hydrological cycle they represent. Importantly, drought indices are proxies rather than direct measurements of drought impacts. Single-variable indices, such as the SPI, characterize meteorological drought solely on the basis of precipitation anomalies (McKee et al., 1993). Multi-variable indices, such as the SPEI, extend this framework by incorporating atmospheric evaporative demand through a climatic water balance, thereby accounting for both water supply and temperature-related moisture loss (Vicente-Serrano et al., 2010). Previous studies have shown that multi-variable indices can produce drought patterns that differ from precipitation-only metrics, particularly in water-limited and warming environments (Sharafi and Ghaleni, 2023; Kumar et al., 2024).

Increasing attention has been given to the role of atmospheric evaporative demand in the development and its impacts (e.g. Ogunrinde et al., 2025; Gebrechorkos et al., 2025). Evaporative demand, commonly represented by ET_o, integrates the effects of air temperature, humidity, wind speed, and solar radiation on the atmosphere's capacity to remove moisture from the land surface. Elevated ET_o can accelerate soil moisture depletion and intensify vegetation stress even when precipitation deficits are moderate (Vicente-Serrano et al., 2015). This process is particularly relevant in arid and semi-arid regions, where water availability is limited, and evapotranspiration (ET) is strongly constrained by soil moisture. Excluding evaporative demand from drought assessments may therefore underestimate hydroclimatic stress, especially under warming conditions (Sharafi and Ghaleni, 2023; Lovino et al., 2024). The physical justification for considering evaporative demand in drought analysis lies in the coupling between land-surface water availability and the atmospheric energy balance. This coupling is formalized by the Budyko framework, which describes how long-term ET is partitioned between water-limited and energy-limited regimes as a function of climatic aridity (Budyko, 1974; Donohue et al., 2011). In energy-limited environments, ET is primarily constrained by available energy, and atmospheric demand responds weakly to changes in soil moisture. In contrast, in water-limited environments—characteristic of many arid regions—ET is constrained by soil moisture availability, and strong feedbacks exist between surface drying and atmospheric conditions.

Under water-limited conditions, declining soil moisture suppresses actual ET, leading to increased sensible heat flux, higher near-surface air temperatures, reduced humidity, and enhanced vapor pressure deficits. These processes increase atmospheric evaporative demand despite reduced surface water availability. Consequently, anomalies in evaporative demand can reflect land-surface drying through their response to changes in surface energy partitioning. Although evaporative demand does not directly represent water availability, its variability is physically linked to surface moisture conditions through land–atmosphere feedbacks. This linkage provides the conceptual basis for interpreting evaporative-demand anomalies as indirect indicators of drought-related stress.

Accurate estimation of evaporative demand requires physically based formulations that incorporate multiple meteorological variables. Simplified temperature-based approaches may introduce uncertainty by neglecting the effects of radiation, humidity, and wind speed (Amani and Shafizadeh-Moghadam, 2023). Comprehensive formulations, such as those based on the Penman–Monteith framework, provide more physically consistent estimates of ET_o and are increasingly used in drought studies to capture climate-driven changes in atmospheric demand (Vicente-Serrano et al., 2015).

In addition to gradual drought development, increasing attention has been given to rapid-onset droughts, commonly referred to as flash droughts. Flash droughts are characterized by a rapid intensification of moisture stress over weeks to months, driven by the combined effects of precipitation deficits and anomalously high evaporative demand associated with elevated temperature, wind speed, and solar radiation (McEvoy et al., 2016a; Christian et al., 2021). These events can cause rapid declines in soil moisture and vegetation condition, resulting in substantial agricultural losses during critical growing periods (Lovino et al., 2024). While indices such as SPI and SPEI can be calculated at short timescales, their reliance on precipitation or water balance alone may limit their sensitivity to rapid changes in atmospheric demand that precede observable precipitation anomalies (Han and Singh, 2023).

The EDDI was developed to quantify standardized anomalies in atmospheric evaporative demand as an indirect indicator of drought-related stress (Hobbins et al., 2016). EDDI is based on anomalies in ET_o and reflects atmospheric conditions that promote enhanced moisture loss from soils and vegetation. It does not directly measure water availability but captures the atmospheric response to land-surface drying and energy-balance changes. Previous studies have demonstrated that EDDI can characterize drought evolution across multiple timescales and may provide early indications of drought development in regions, such as the United States and East Asia (Zhang et al., 2017; Ng et al., 2024). Forecast studies have also shown that evaporative demand is more predictable can exhibit higher predictability than precipitation at seasonal timescales, supporting its relevance for drought preparedness (McEvoy et al., 2016b).

Despite these advances, the behavior of evaporative-demand-based drought indicators in arid regions remains insufficiently examined. Arid Asia and Africa are characterized by highly variable precipitation, high evaporative demand, and limited soil-moisture buffering capacity. In such environments, drought signals may be particularly sensitive to sub-seasonal variability in atmospheric demand (Christian et al., 2021). While drought characteristics in these regions have been widely studied using precipitation- and water-balance-based indices (e.g., Shawaqfeh et al., 2025; Wu et al., 2024; Ogunrinde et al., 2024a), fewer studies have assessed how evaporative-demand-based indices relate to these traditional measures across timescales.

This study examines drought dynamics in arid regions of Asia and Africa using EDDI alongside SPI and SPEI derived from consistent ERA5 data. The analysis compares spatial and temporal drought patterns, trend characteristics, and inter-index relationships across multiple timescales, with emphasis on extreme and rapid-onset drought events. By framing these indices as complementary indicators grounded in the physical linkage between land-surface water availability and atmospheric energy balance, the study aims to improve understanding of drought processes in arid environments and to inform multi-index drought-monitoring and early-warning applications.

2. Methodology

2.1. Study area

The study area spans arid regions of Asia and Africa, encompassing diverse IPCC-classified zones: Sahara (SAH), Mediterranean (MED), Arabian Peninsula (ARP), West Central Asia (WCA), Eastern Europe (EEU), West Siberia (WSB), East Siberia (ESB), East Central Asia (ECA), and Tibetan Plateau (TIB). The geographic coordinates range from approximately 10 to 50° N latitude and 15 to 125° E longitude (Fig. 1). These regions are home to many countries with similar climatic and environmental challenges. Topographically, the region varies significantly, with elevations ranging from −433 m in low-lying areas to 8 564 m in the TIB, influencing local climates and drought patterns. Vegetation, as depicted in the land use land cover map (Fig. 1), is predominantly sparse, with large expanses of barren land and savannas, particularly in SAH and ARP. Grasslands and permanent wetlands are scattered, whereas croplands and natural vegetation mosaics are present in the WCA and ECA. Evergreen and deciduous forests are minimal, mostly in EEU and ESB, reflecting the arid climate's dominance.

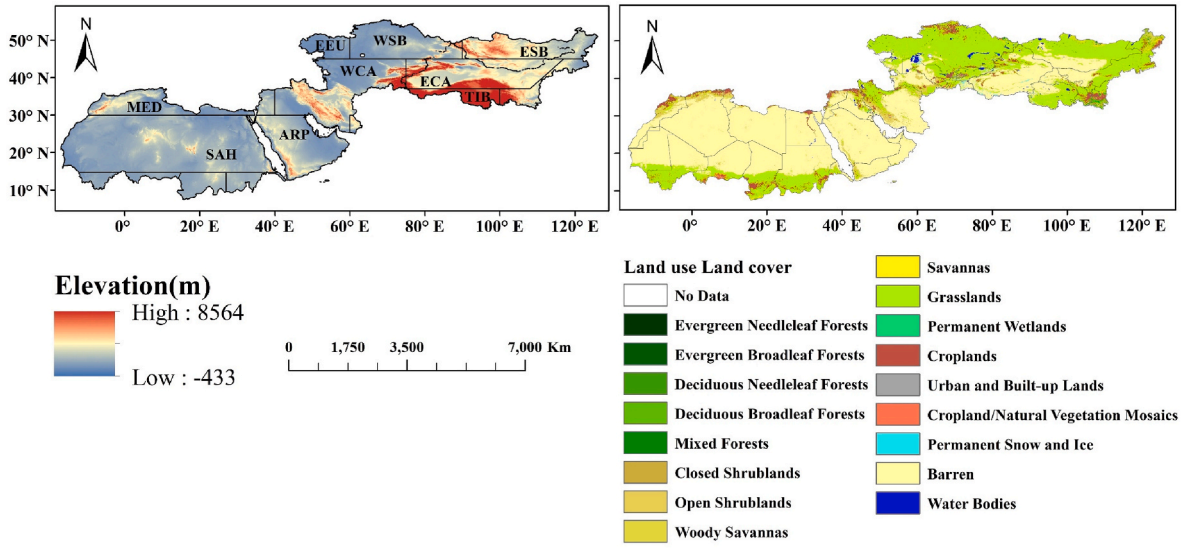

Fig. 1. Map of the study area showing (a) the elevation and the IPCC classification: SAH- Sahara; MED – Mediterranean; ARP – Arabian Peninsula; WCA – West Central Asia; EEU – Eastern Europe; WSB – West Siberia; ESB - East Siberia; ECA – East Central Asia; TIB – Tibetan-Plateau (b) the Land use Land Cover map with country boundaries.

2.2. Data

In this study, five key atmospheric variables—precipitation, surface mean air temperature, dewpoint temperature, surface net solar radiation, and wind speed—were analyzed using the ERA5 land reanalysis datasets developed by the European Centre for Medium-Range Weather Forecasts (ECMWF). The ERA5 dataset, with its high spatial resolution of $0.1^\circ \times 0.1^\circ$, has been widely recognized for its accuracy and reliability in representing climatic conditions, particularly in data-scarce regions, when compared to other global reanalysis datasets (Al-Sakkaf et al., 2024; Clelland et al., 2024; Hou et al., 2023). For arid regions, ERA5 has proven effective in capturing rainfall variability and temperature extremes, which are critical for understanding drought dynamics and water resource challenges. Supplementary Fig. S1 and S2 demonstrated strong correlations between ERA5 data and ground-based observations in arid zones. Al-Sakkaf et al. (2024) found high agreement between ERA5 rainfall data and station observations across the ARP, while Hou et al. (2023) highlighted its accuracy in representing temperature and radiation patterns in Central Asia. Such findings underscore the suitability of ERA5 for climate analysis in these regions, where ground-based meteorological networks are sparse or inconsistent. The ERA5 reanalysis datasets were extracted based on their spatial resolution to encompass the entire study area from 1983 to 2023. The daily ET_o was calculated using the Penman-based ASCE standardized equation (ASCE, 2005):

$$ET_0 = \frac{0.408\Delta(Rn - G) + \gamma \frac{C_n}{T+273} u_2 (e_s - e_a)}{\Delta + \gamma(1 + C_d u_2)} \quad (1)$$

$$e^o(T) = 0.6108 \exp\left[\frac{17.27T}{T + 237.3}\right] \quad (2)$$

$$e_s = \frac{e^o(T_{max}) + e^o(T_{min})}{2} \quad (3)$$

$$e_a = e^o(T_{dew}) = 0.6108 \exp\left[\frac{17.27T_{dew}}{T_{dew} + 237.3}\right] \quad (4)$$

Where, ET_0: reference evapotranspiration; Δ: Slope of the saturation vapor pressure-temperature curve (kPa $^\circ C^{-1}$), R_n: Net radiation at the crop surface (MJ m^{-2} d^{-1}), G: Soil heat flux density at the soil surface (MJ m^{-2} d^{-1}), typically set to 0 for daily estimates, γ: Psychrometric constant (kPa $^\circ C^{-1}$), T: mean air temperature (°C), u: Wind speed at 2 m height (m s^{-1}), e_s - e_a: Vapor pressure deficit (kPa), C_n: numerator constant for reference type and daily calculation time step (900), C_d: denominator constant for reference type and daily calculation time step (0.34), 0.408: Conversion factor for ET_0 into mm d^{-1}. The methodology for calculating relative humidity from dewpoint temperature and mean air temperature is detailed in the FAO-56 publication (Allen et al., 1998).

2.3. Drought indices

2.3.1. Evaporative Demand Drought Index (EDDI)

In this study, we computed EDDI using the methodology proposed by Hobbins et al. (2016). Gridded ET_0 data were aggregated over 1-, 2-, and 3-week timescales, as well as 1-, 3-, 6-, and 12-month accumulation periods, allowing the characterization of drought conditions from short-term to longer-term contexts. These timescales enable assessment of both rapid-onset and persistent drought conditions. For each grid cell and accumulation period, aggregated ET_0 values were ranked and converted to empirical cumulative probabilities using a nonparametric approach. Empirical probabilities were estimated using the Tukey plotting position method (Wilks, 2011), thereby avoiding assumptions about the underlying statistical distribution of ET_0. The cumulative probabilities were subsequently transformed into standardized normal deviates using the inverse normal approximation method described by Abramowitz and Stegun (1965), yielding EDDI values with a mean of zero and unit variance. A value of zero corresponds to median atmospheric evaporative demand, while positive values indicate anomalously high evaporative demand and negative values indicate anomalously low demand. Positive EDDI values are interpreted as conditions conducive to

Table 1
Classification of drought severity levels for SPI, SPEI and EDDI.

Category	Drought intensity	EDDI	SPEI and SPI
C0	No drought	−0.5 – 0.5	−0.5 – 0.5
C1	Mild drought	0.5 – 1.0	−1.0 to −0.5
C2	Moderate drought	1.0 – 1.5	−1.5 to −1.0
C3	Severe drought	1.5 – 2.0	−2.0 to −1.5
C4	Extreme drought	≥2.0	≤ −2.0

Note: Categories follow conventional thresholds used for SPI/SPEI (McKee et al., 1993; Vicente-Serrano et al., 2010) and applied to EDDI by Ng et al. (2024).

drought development (Table 1).

Although EDDI does not directly represent water availability, it provides an indirect proxy for drought-related stress through its linkage to land–atmosphere interactions. The physical basis for this proxy is grounded in the coupling between surface moisture conditions and the atmospheric energy balance, as described by the Budyko framework (Budyko, 1974; Donohue et al., 2011). In water-limited environments, such as arid and semi-arid regions, declining soil moisture suppresses actual evapotranspiration, leading to increased sensible heat flux, higher near-surface air temperatures, lower humidity, and increased vapor pressure deficits. These changes enhance atmospheric evaporative demand despite reduced surface water availability. Consequently, anomalies in ET_0 reflect the atmospheric response to land-surface drying and energy partitioning, making EDDI a physically meaningful, albeit indirect, indicator of drought processes. In this study, EDDI is therefore interpreted as complementary to precipitation- and water-balance-based indices rather than as a direct measure of water deficit.

2.3.2. Standardized Precipitation Index (SPI) and Standardized Precipitation Evapotranspiration Index (SPEI)

For comparison, the SPI and SPEI were computed at 1-, 3-, 6-, and 12-month timescales. SPI was calculated from precipitation data fitted to a gamma distribution and transformed to a standardized normal distribution (McKee et al., 1993). SPEI was computed following Vicente-Serrano et al. (2010), based on the climatic water balance between precipitation and ET_0, with the resulting series fitted to a log-logistic distribution and standardized. Negative SPI and SPEI values indicate dry conditions, while positive values indicate wet conditions. Following Ng et al. (2024), drought severity for SPI, SPEI, and EDDI was classified into five categories ranging from no drought (C0) to extreme drought (C4), as summarized in Table 1.

2.4. Assessment approach

To assess temporal trends in SPI, SPEI, EDDI, and associated climate variables, a rank-based Mann–Kendall test was applied. This nonparametric approach is well-suited for detecting monotonic trends in hydroclimatic time series and is robust to non-normality and outliers. To account for serial correlation, the modified Mann–Kendall test proposed by Hamed and Ramachandra Rao (1998) was used. Trend magnitude was quantified using Sen's slope estimator, which provides a median rate of change. Relationships among SPI, SPEI, and EDDI were evaluated using Spearman's rank correlation coefficient at a 5% significance level. This statistic ranges from −1 to 1, representing perfect negative and positive monotonic association. In addition, a case study of a severe drought event was conducted to examine drought evolution at 1-, 3-, 6-, and 12-month timescales, enabling comparison of index behavior for drought detection and operational relevance.

2.5. Drought characterization

Drought characteristics were quantified using the run theory originally proposed by Yevjevich (1967), which is widely applied to identify and characterize drought events in time series of standardized indices. A drought event is defined as a continuous sequence of values that remain below a predefined threshold (e.g. −1 as used in the current study), thereby forming a "run" (Guo et al., 2018; Ogunrinde et al., 2024c). This framework is appropriate because sustained negative index values are associated with cumulative stress on vegetation, crops, and ecosystems, and support early detection of drought development (Sheffield et al., 2012). Using run theory, several drought attributes were derived. Average duration (AD) represents the mean length of drought events, measured as the number of consecutive months below the threshold. Frequency (F) denotes the total number of drought events during the study period. Average severity (AS) is calculated as the mean cumulative sum of index values during drought events, reflecting total moisture deficit. Average intensity (AI) is defined as the ratio of severity to duration and represents the mean deficit per month. Average peak (AP) corresponds to the most negative index value within each drought event, indicating maximum drought intensity. These variables are detailed in prior studies (Mishra and Singh, 2010; Guo et al., 2018).

$$AD = \frac{\sum_{i=1}^{N} D_i}{N} \ (month) \tag{5}$$

$$AS = \frac{\sum_{j=1}^{N} S_j}{N}, S = \sum_{i=1}^{D} |EDDI_i| \tag{6}$$

$$AI = \frac{\sum_{j=1}^{N} I_j}{N}, I = \frac{\sum_{i=1}^{D} |EDDI_i|}{D} \tag{7}$$

$$AP = \frac{\sum_{j=1}^{N} P_j}{N}, P = \max_{1 \le i \le D} |EDDI_i| \tag{8}$$

3. Results

3.1. Spatial patterns of climatic conditions relevant to drought

Fig. 2 illustrates the spatial distribution of long-term monthly mean climatic variables across the arid regions of Asia and Africa for the period 1983–2023. These spatially averaged variables provide a quantitative characterization of prevailing climatic conditions within which drought indices are evaluated. The variables shown—ET_o, precipitation, mean air temperature, wind speed, solar radiation, and relative humidity—collectively describe the atmospheric and surface environment across the study domain. ET_o, employed here as an indicator of atmospheric evaporative demand, exhibits pronounced spatial heterogeneity. Mean monthly ET_o values exceed 150 mm $month^{-1}$ across large portions of the ARP, the SAH, and parts of western Asia, reflecting persistently high evaporative demand typical of hyper-arid environments (Allen et al., 1998; Ogunrinde et al., 2024b). In contrast, substantially lower ET_o values occur at higher latitudes and over elevated terrain, including WSB, ESB, and the TIB, where cooler climatic conditions prevail.

Mean precipitation displays a contrasting spatial pattern, with monthly averages below 50 mm across extensive areas of SAH and ARP, consistent with their classification as hyper-arid regions. Higher mean precipitation amounts are observed in regions such as EEU, WSB, and portions of TIB, highlighting pronounced spatial gradients in moisture availability across the broader arid-domain classification. Mean monthly air temperature follows a largely latitudinal and elevational structure, with values exceeding 30 °C concentrated in low-latitude desert interiors and progressively lower values toward higher latitudes and at higher elevations. Additional climatic variables further differentiate regional settings. Mean wind speeds greater than 4 m s^{-1} are characteristic of exposed desert and steppe regions, including parts of SAH and WCA, while lower values are associated with more topographically complex areas. Solar radiation generally exceeds 20 MJ m^{-2} day^{-1} across low-latitude arid zones, whereas relative humidity frequently falls below 40% over SAH and ARP and is comparatively higher in regions influenced by elevation or seasonal moisture transport. These spatially averaged climatic variables establish the environmental context against which drought indices reflecting different sensitivities to atmospheric demand and moisture availability are examined in subsequent analyses.

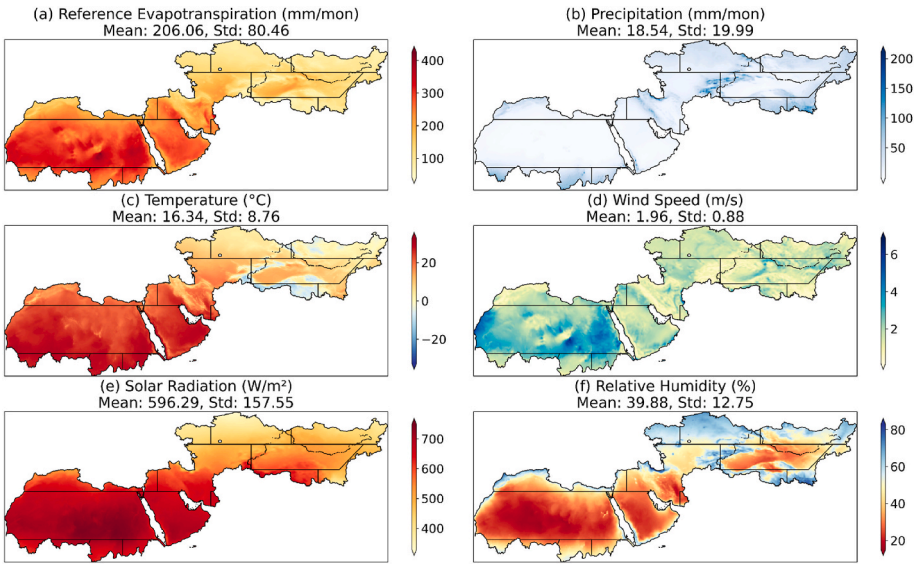

Fig. 2. Spatial distribution of monthly average (a) reference evapotranspiration (ET_o), (b) precipitation, (c) Mean temperature, (d) wind speed, (e) solar radiation, and (f) relative humidity over Arid Regions of Asia and Africa during 1983–2023.

3.2. Spatial trends and climatic influences on drought indices

Fig. 3 presents the annual trends in the SPI, SPEI, and EDDI at 1-, 3-, 6-, and 12-month timescales, along with the degree of agreement among these indices. The figure shows wetting and drying trends as a function of the level of temporal aggregation. Among the indices, spatial agreement is greater at shorter timescales, while differences increase at longer timescales. At longer timescales, the magnitudes of both drying and wetting trends generally increase, except for the ARP, which exhibits consistent drying across all timescales. This increase arises from the accumulation of hydroclimatic anomalies over extended periods, during which short-term variations result in prolonged deficits or surpluses. This process is consistent with the cumulative nature of drought propagation. Notably, EDDI delineates more acute drying trends throughout the study area than SPI and SPEI, especially in SAH, MED, and segments of WCA, attributable to its exclusive focus on the evaporative demand estimate, which captures atmospheric thirst independent of precipitation inputs (Hobbins et al., 2016).

Regional overlaps in trend patterns are apparent in EEU, WSB, ECA, ESB, WCA, and portions of ARP, signifying aligned responses to shared climatic forcings. In contrast, the TIB and central SAH exhibit pronounced discrepancies: SPI and SPEI indicate significant wetting, potentially linked to episodic precipitation enhancements, whereas EDDI registers nonsignificant drying, underscoring the overriding influence of ET_o in these locales, driven by elevated temperatures and diminished humidity that eclipse moisture gains. This index-specific divergence illuminates methodological nuances—SPI's precipitation-only lens may overlook ET_o-driven desiccation, while SPEI's hybrid

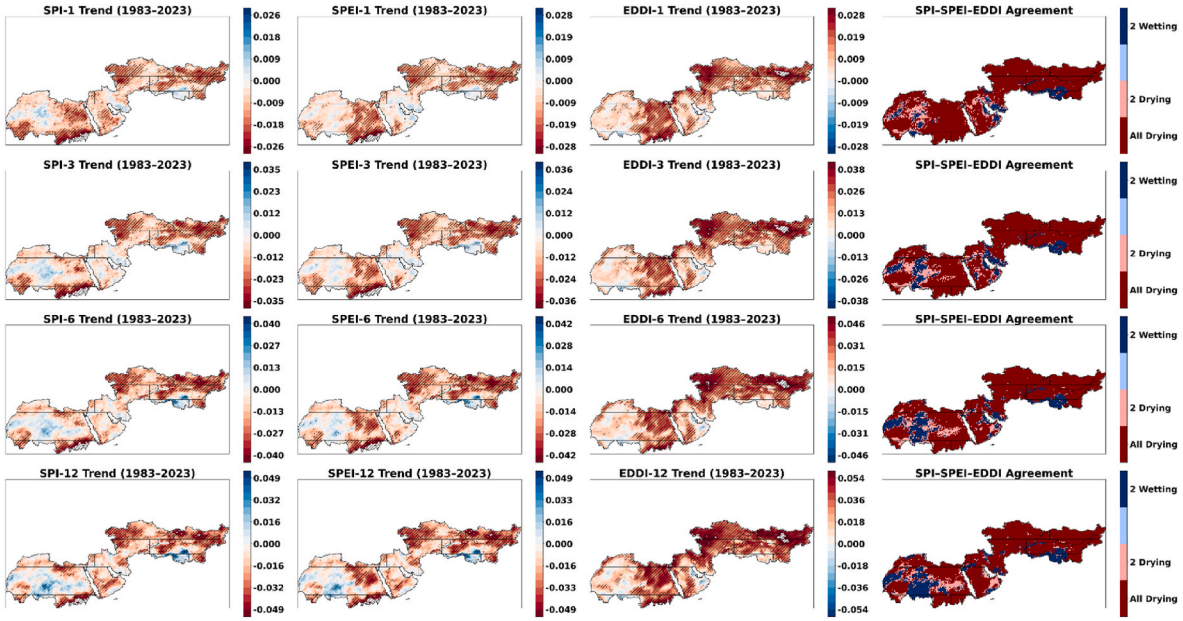

Fig. 3. Spatial distribution of annual trends (1983–2023) in drought indices across multiple timescales. Panels show trends of the Standardized Precipitation Index (SPI), Standardized Precipitation Evapotranspiration Index (SPEI), and Evaporative Demand Drought Index (EDDI) at 1-month (first row), 3-month (second row), 6-month (third row), and 12-month (fourth row) timescales. The rightmost panels illustrate the spatial agreement among SPI, SPEI, and EDDI in identifying wetting and drying trends.

approach yields intermediate signals that balance supply and demand, thereby underscoring the necessity of complementary indices in arid assessments.

Complementing these patterns, Fig. 4 quantifies the areal proportions of grid cells across IPCC-defined regions (as in Fig. 1) stratified into five trend categories: significant drying, nonsignificant drying, no trend, nonsignificant wetting, and significant wetting. This granular breakdown reveals stark regional heterogeneities, with EDDI showing pervasive, significant drying across timescales, encapsulating the escalating role of evaporative demand in a warming world (Dai, 2013). In EEU and ESB, over 70% of grid cells fall into the significant drying class, consistent with proposed mechanisms of mid-latitude amplification, in which rising temperatures and altered circulation patterns may heighten ET_o through influences on vapor pressure and radiation fluxes, as emphasized in Penman-Monteith formulations (Allen et al., 1998). The TIB, by contrast, exhibits subdued drying (<10% significant under EDDI), potentially consistent with the proposed effects of altitudinal buffering and/or orographic precipitation, which may mitigate evaporative losses (Immerzeel et al., 2020). Here, SPI and SPEI allocate 25–35% to significant wetting, with the balance spanning nonsignificant drying, neutral, and wetting categories, potentially reflecting the plateau's complex interplay of cryospheric and monsoonal influences. Intermediate profiles characterize MED, ARP, and SAH, where EDDI assigns 45-60% to significant drying, juxtaposed with SPI/SPEI's modest wetting (10-18%), highlighting differential sensitivities to precipitation versus ET_o drivers (Vicente-Serrano et al., 2020). WCA and WSB further accentuate contrasts, with EDDI indicating 70-100% significant drying amid intensified evaporative stress, while SPI/SPEI caps at 20-50%. These quantifications not only reinforce the spatial mosaics in Fig. 3 but also advocate for region-tailored monitoring strategies that integrate evaporative perspectives to avoid underestimating aridification risks.

Underpinning these trends, Fig. 5 maps spatial patterns in climatic variables from 1983 to 2023, with hatched zones denoting statistical significance at the 5% level. ET_o (Fig. 5a) shows robust positive trends (2.0 to 5.16 mm/year) in EEU, WSB, ESB, and the SAH, WCA, and ECA sectors, corroborating the drying signals in Fig. 3 and implicating warming-induced demand surges. TIB counters with a negative trend (−1.0 mm/year), likely driven by high-elevation cooling and enhanced cloudiness, which dampen evaporation (IPCC, 2021). Precipitation (Fig. 5b) inversely correlated to ET_o, with TIB showcasing the most vigorous positive increments, indicative of a localized hydrological surplus amid broader aridity. Mean temperature (Fig. 5c) ascends significantly (0.02 to 0.05 °C/year), peaking in SAH, ARP, and WCA, where it synergistically boosts ET_o via increased saturation deficits. Wind speed (Fig. 5d) lacks cohesive patterning, though positive (nonsignificant) trends dominate, marginally augmenting aerodynamic contributions to ET_o. Solar radiation (Fig. 5e) trends upward (non-significantly) north of 45°N (e.g., WSB, ESB), but significantly downward southwards, especially in SAH and TIB, possibly due to aerosol dimming or convective cloud feedbacks (Wild, 2009). Relative humidity (Fig. 5f) declines significantly east of 60°E (e.g., ARP, ESB), with milder drops westward, except TIB's subtle rises that align with its precipitation upticks. These drivers elucidate the mechanistic foundations of observed drought trends, emphasizing ET_o's central role in arid-climate trajectories.

3.3. Temporal dynamics and correlations of drought indices

Fig. 6 presents the averaged time series of the EDDI, SPI, and SPEI for the ARP, SAH, MED, and TIB regions from 1983 to 2023. Supplementary Fig. S3 provides equivalent time series for the ECA, ESB, EEU, WCA, and WSB regions. The three indices exhibit strong coherence, particularly at

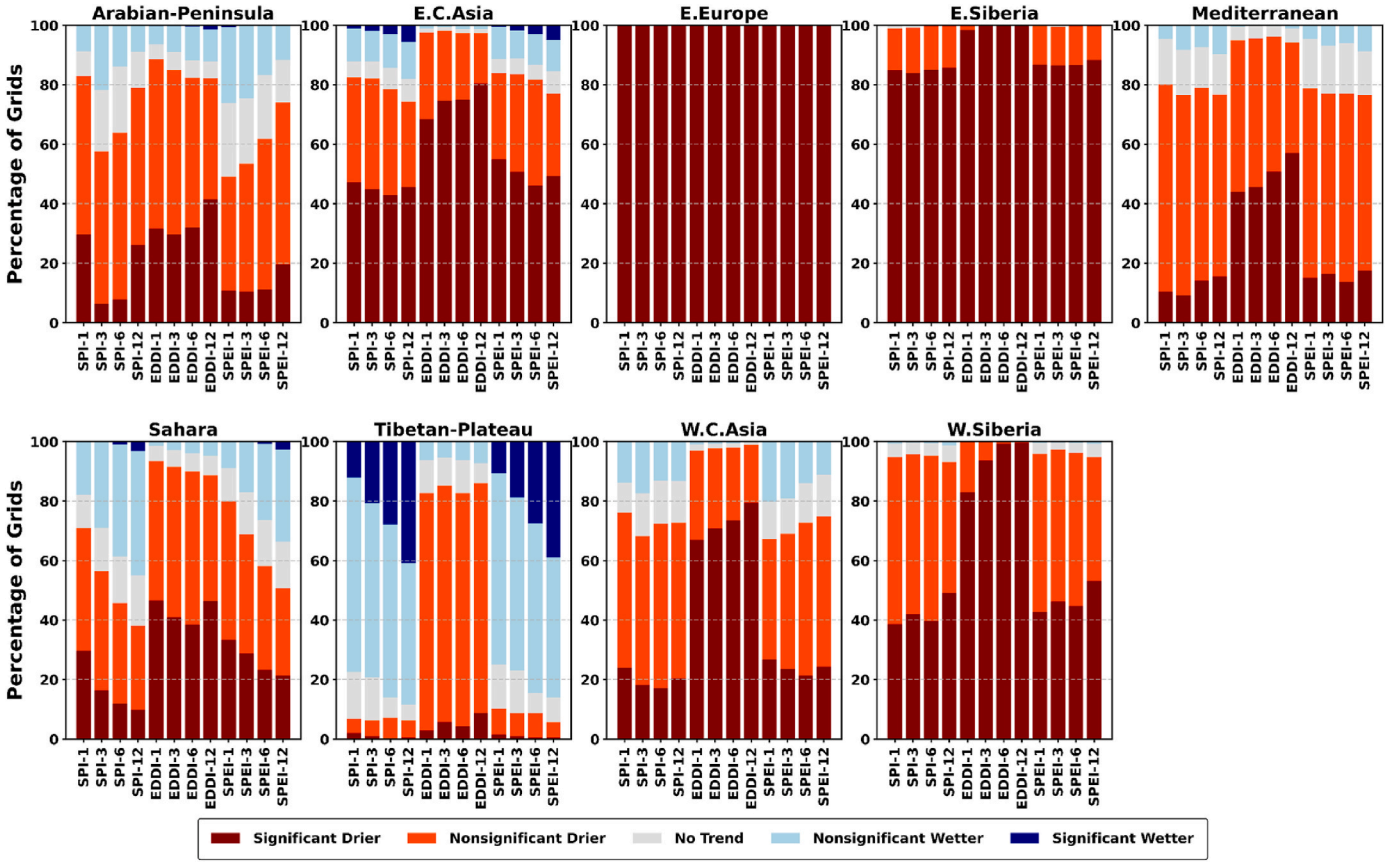

Fig. 4. The proportion of grid cells categorized into five trend classes—significant drier, nonsignificant drier, no trend, nonsignificant wetter, and significant wetter—was analyzed individually for each region.

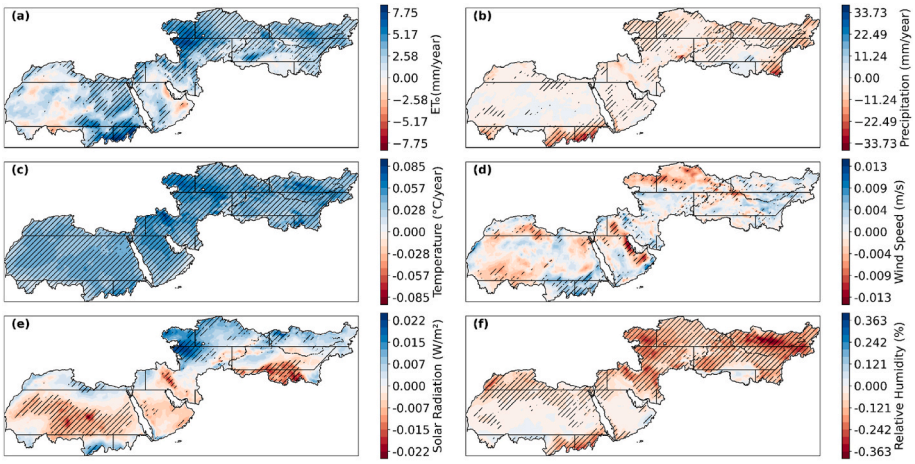

Fig. 5. Spatial patterns of trends in (a) reference evapotranspiration (ET_o), (b) precipitation, (c) mean temperature, (d) wind speed (e) solar radiation, and (f) relative humidity across the study area from 1983 to 2023. Hatch marks areas with statistical significance at a 5% level.

the 6- and 12-month timescales, where EDDI closely aligns with drought episodes identified by SPI and SPEI. This alignment reflects their shared sensitivity to sustained hydroclimatic drivers. At the 1-month timescale, greater variability is evident, with more pronounced peaks and troughs that respond to short-term anomalies in precipitation or ET_o. Longer accumulation periods produce smoother time series, revealing decadal-scale variability that captures the cumulative nature of drought development (Vicente-Serrano et al., 2020). Since 2000, drought frequency has increased in all regions except TIB, consistent with accelerated global aridification under anthropogenic warming (UNCCD, 2024). Notable drought events include the 1998–2000 and 2010–2012 episodes in ARP, the 1983–1985 and 2001–2003 episodes in SAH, and the 2007–2008 event in WCA. Multi-year droughts of greater intensity have occurred after 2000 in ARP, EEU, ESB, and WSB. The 2001–2002 drought in ARP and SAH exhibited higher EDDI magnitudes than SPI or SPEI, due to the dominant role of elevated ET_o in amplifying aridity in these regions (Hobbins et al., 2016).

Fig. 7 illustrates the correlations (Spearman's ρ) between EDDI and SPI, and between EDDI and SPEI, across multiple timescales. Significant correlations ($p < 0.05$) are indicated by hatching. Numerical values for sub-regions are provided in Table 2, where all correlations are significant at the 5% level. Negative ρ values indicate opposing signs between the indices: EDDI increases with higher atmospheric evaporative demand, while SPI and SPEI decrease during precipitation deficits. Correlations are generally strong ($\rho < -0.61$), but EDDI–SPI associations weaken and EDDI–SPEI associations strengthen with increasing timescale. Examples include ARP values ranging from −0.90 (EDDI–SPEI, 1-month) to −0.79 (EDDI–SPI, 12-month), MED from −0.83 (EDDI–SPEI, 1-month) to −0.69 (EDDI–SPI, 1-month), and ESB from −0.84 (EDDI–SPEI, 12-month) to −0.83 (EDDI–SPI, 12-month). Weaker correlations occur in WSB (−0.43 to −0.72) and TIB (−0.41 to −0.47), indicating regional differences in index coupling. Spatially, the strongest EDDI–SPEI correlations ($\rho < -0.8$) are concentrated in SAH, MED, and ARP, consistent with Table 2 and the climatic patterns shown in Fig. 5. EDDI–SPI correlations are weaker in SAH and TIB (−0.3 to −0.6), with spatially discontinuous significance likely due to low precipitation and topographic heterogeneity. These results confirm the complementary value of EDDI for improving drought characterization across diverse climatic regimes.

3.4. Spatial patterns of drought characteristics

Fig. 8 and Supplementary Figs. 11 and 12 present the spatial distributions of drought characteristics—average duration, severity, intensity, peak, and frequency—derived from EDDI, SPEI, and SPI across multiple timescales. These distributions highlight differences among the indices that arise from their respective sensitivities to hydroclimatic variables. Average duration (first-row panels) increases with timescale, consistent with the progression of drought from meteorological to hydrological stages as deficits affect subsurface storage and reservoirs (Van Loon, 2015). Average severity and intensity (second- and third-row panels) also increase with timescale, reflecting the compounding effects of persistent anomalies. In contrast, average peak and frequency (fourth- and fifth-row panels) decrease at longer timescales for SPI and SPEI due to the normalizing effect of extended accumulation periods on anomalies. EDDI shows greater severity in the SAH and ARP regions, attributable to the strong influence of ET_o. Conversely, SPI emphasizes higher drought frequencies driven by precipitation variability in the TIB. These index-specific patterns underscore the value of multi-index approaches for comprehensive drought characterization and the development of effective adaptation strategies in arid regions.

3.5. Temporal sensitivity and drought progression

Fig. 9 presents the temporal evolution of EDDI at timescales ranging from 2 weeks to 12 months in the ARP, WCA, and SAH regions for the period 1983–2023, with Supplementary Fig. S4–S9 providing equivalent results for the remaining regions. At sub-weekly timescales, EDDI reflects the drought episodes identified in Fig. 6 (e.g., 1994–1996, 2006–2007, and 2015–2022 in ARP; 2006–2022 in WCA), but exhibits greater variability in response to rapid atmospheric perturbations. At longer timescales, intensified drought extremes are evident after 2000, particularly the prolonged 2009–2022 event in ARP, which corresponds to increases in ET_o (Fig. 5a). Fig. 10 examines the sub-seasonal development of EDDI during the 2010 drought across the eight regions. At short timescales (1–4 weeks), EDDI increases precede the 3-month peaks, indicating earlier drought onset in ARP and SAH relative to SPI (Fig. 11). Rapid intensification is observed in ECA and ESB, while MED and TIB display more moderate responses associated with moisture supply. This sensitivity at sub-monthly timescales supports the utility of EDDI for monitoring flash droughts driven by rapid increases in ET_o.

Drought severity increases with accumulating timescale, with the extreme drought category (C4) becoming more prominent, particularly for EDDI and SPEI compared to SPI across all timescales (Fig. S10a–c). The C4 category is most evident in SAH and ARP during January and February, associated with sustained elevated ET_o and low precipitation (Fig. 5). At longer timescales, EDDI and SPEI identify moderate-to-severe drought categories (C1–C3) across parts of the study area, reflecting accumulated precipitation deficits. At the 1-month timescale (Fig. 11), EDDI and SPEI indicate mild-to-severe drought mainly in SAH

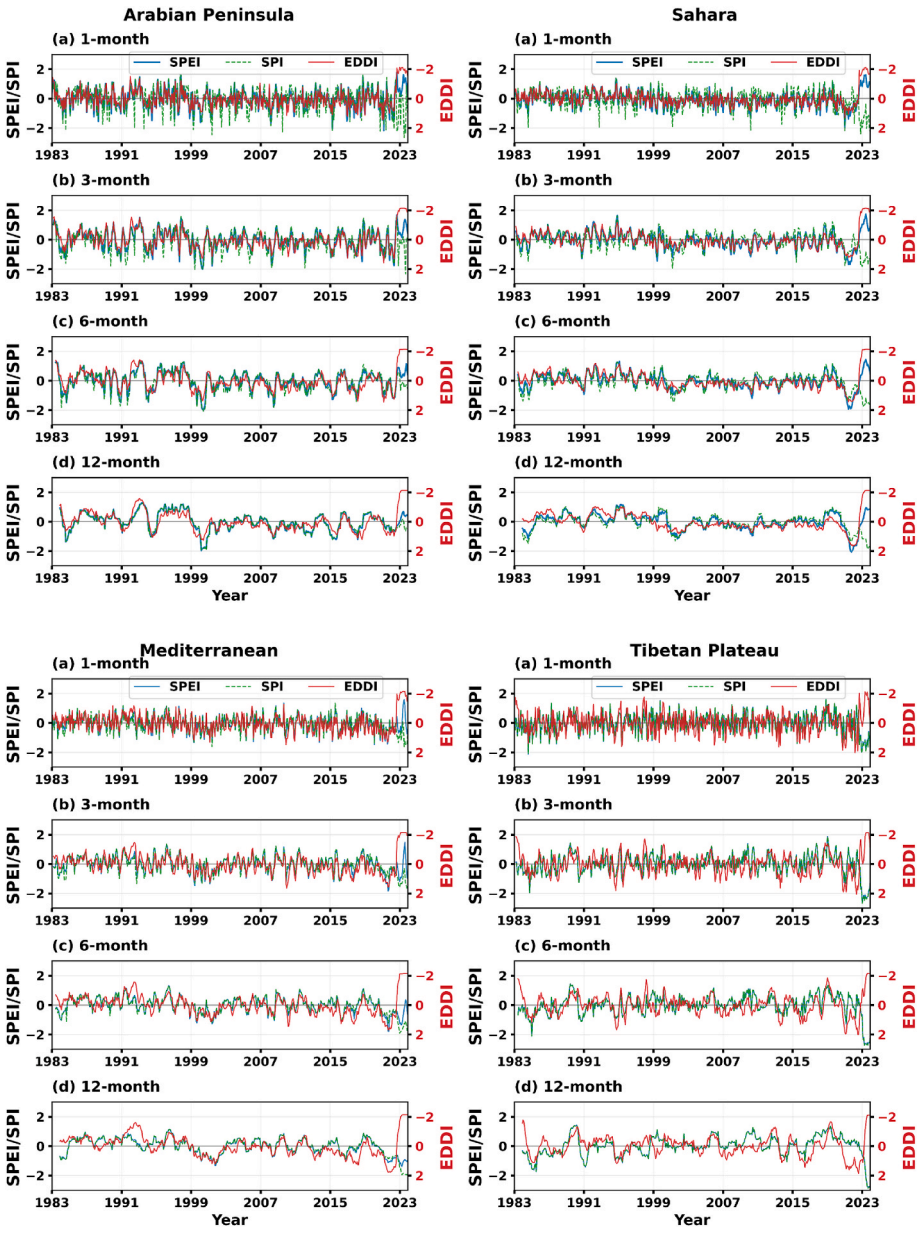

Fig. 6. Time-series fluctuations of drought indices, averaged regionally, for Arabian Peninsula (ARP), Sahara (SAH), Mediterranean (MED), and Tibetan Plateau (TIB) regions over the period 1983–2023. The EDDI y-axes are reversed to reflect the inverse relationship between EDDI and the SPI and SPEI indices.

and ARP, with localized occurrences in WCA during January–February 2010. The severity indicated by SPEI-1 aligns more closely with EDDI than with SPI-1, consistent with the influence of ET_o in the early phase. On the 3-month timescale (Fig. S10a), EDDI and SPEI show expansion of severe drought in ARP and SAH, persisting until May 2010, whereas SPI-3 and SPEI-3 exhibit a delay and capture broader areas in WCA related to precipitation anomalies (Fig. 5b). At the 6- and 12-month timescales (Fig. S10b and c), all indices reach peak severity (e.g., C4 in parts of EEU and SAH), but EDDI signals drought onset earlier than SPI and SPEI by several weeks in central to eastern SAH, while SPI maintains more limited spatial coverage. This earlier detection by EDDI is consistent with its sensitivity to ET_o, which responds to atmospheric drying prior to precipitation-based indices.

4. Discussion

4.1. Drought index performance and climatic drivers in arid environments

The comparison of drought indices in this study indicates performance differences under arid-region hydroclimatic conditions in Asia and Africa, where EDDI identifies more severe drying trends than SPI and SPEI. This difference results from EDDI's dependence on ET_o, which is the primary driver of moisture deficits in regions where atmospheric evaporative demand exceeds precipitation inputs (Hobbins et al., 2016). In hyper-arid regions such as the SAH and ARP, EDDI shows significant drying in 45–60% of grid cells, even when SPI indicates wetting conditions. This difference arises from the index formulations, with EDDI emphasizing ET_o anomalies rather than precipitation alone. These results are consistent with observations in North Africa, where SPEI indicates increased drying despite stable precipitation, highlighting the role of ET_o in arid-drought processes (Tanarhte et al., 2024). Climatic trends contribute to these differences in index performance, as shown in

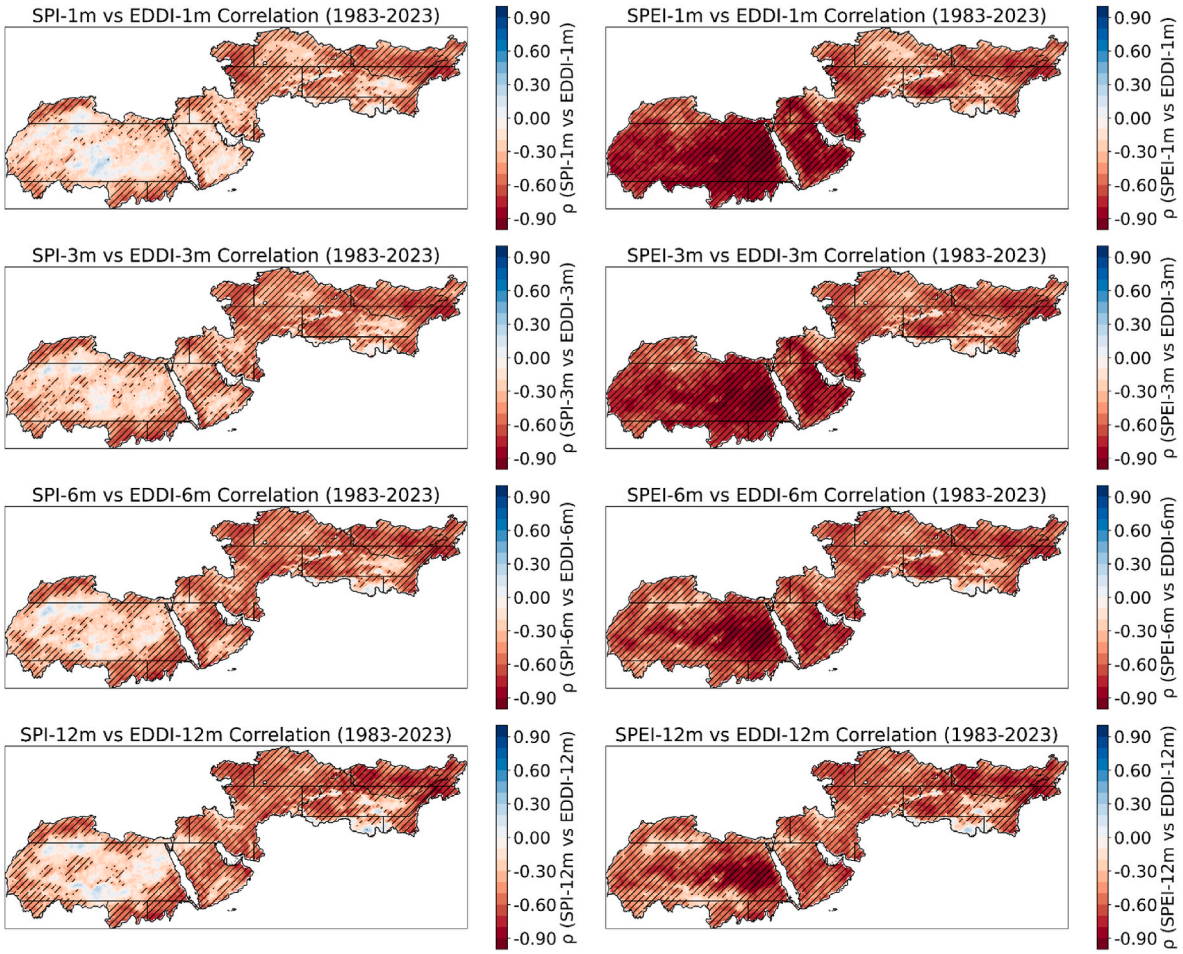

Fig. 7. Spatial pattern of correlations between SPI vs EDDI and SPEI vs EDDI among drought indices at 1-month (first-row panels), 3-month (second-row panels), 6-month (third-row panels) and 12-month (fourth-row panels) timescales. Hatch areas indicate statistical significance at a 5 % significance level.

Table 2
Temporal correlations between EDDI and SPI/SPEI for each sub-region within the study area. All results achieve statistical significance at a 5% confidence level.

Regions	Index	Timescales			
		1-month	3-month	6-month	12-month
Arabian Peninsula	SPEI	−0.90	−0.86	−0.82	−0.83
	SPI	−0.64	−0.69	−0.73	−0.79
East Central Asia	SPEI	−0.71	−0.68	−0.70	−0.71
	SPI	−0.62	−0.61	−0.64	−0.67
East Siberia	SPEI	−0.66	−0.75	−0.82	−0.84
	SPI	−0.62	−0.72	−0.80	−0.83
Eastern Europe	SPEI	−0.57	−0.61	−0.69	−0.79
	SPI	−0.55	−0.58	−0.67	−0.74
Mediterranean	SPEI	−0.83	−0.77	−0.72	−0.68
	SPI	−0.69	−0.64	−0.64	−0.63
Sahara	SPEI	−0.91	−0.88	−0.83	−0.72
	SPI	−0.50	−0.57	−0.56	−0.47
Tibetan-Plateau	SPEI	−0.47	−0.47	−0.44	−0.47
	SPI	−0.44	−0.44	−0.41	−0.45
West Central Asia	SPEI	−0.79	−0.76	−0.74	−0.74
	SPI	−0.72	−0.71	−0.69	−0.71
West Siberia	SPEI	−0.43	−0.51	−0.64	−0.72
	SPI	−0.40	−0.47	−0.61	−0.70

Fig. 5. Significant increases in temperature (0.02–0.05 °C year^{-1}) across the study domain, with the highest rates in SAH, ARP, and WCA, drive increases in ET_o (2.0–5.16 mm year^{-1} in EEU, WSB, ESB, and parts of SAH, WCA, ECA). Decreases in relative humidity east of 60°E further increase vapor pressure deficits and soil drying. These trends align with drying signals in EDDI and SPEI (Fig. 3) and explain why precipitation-based indices such as SPI may underestimate drought severity in regions dominated by ET_o variability (Qing et al., 2023). Similar patterns have been reported in northwestern China, corresponding to conditions in WCA, where ET_o dominates precipitation variability (Wang et al., 2017). In contrast, the TIB shows limited drying, with stable ET_o, unchanged humidity, and positive precipitation trends (ET_o decline <1.0 mm year^{-1}), resulting in lower drought frequency across indices (Figs. 3 and 4). These conditions are associated with elevation effects and monsoonal precipitation inputs that reduce evaporative stress (Immerzeel et al., 2020).

Drought frequency and severity have increased after 2000, as indicated by regional time series (Fig. 6 and Supplementary Fig. S3), with the 2010 event showing peak intensity under EDDI and SPEI in ARP and SAH. This reflects the influence of ET_o in hyper-arid regions, where low precipitation and limited soil moisture allow ET_o to sustain moisture deficits (Allen et al., 1998). Although short-term drought stress is often linked to ET_o and longer-term droughts to precipitation-driven subsurface storage (Van Loon, 2015), results here indicate sustained ET_o influence in arid regions. This is supported by projections using SPI and SPEI, which anticipate increased drought severity under warming (Naumann et al., 2018).

Across timescales (Fig. 8a–c), drought duration, severity, and intensity increase with accumulation period, consistent with drought propagation from meteorological to hydrological conditions (Van Loon, 2015). However, EDDI maintains higher values over longer timescales than the declines in SPI and SPEI, reflecting amplification associated

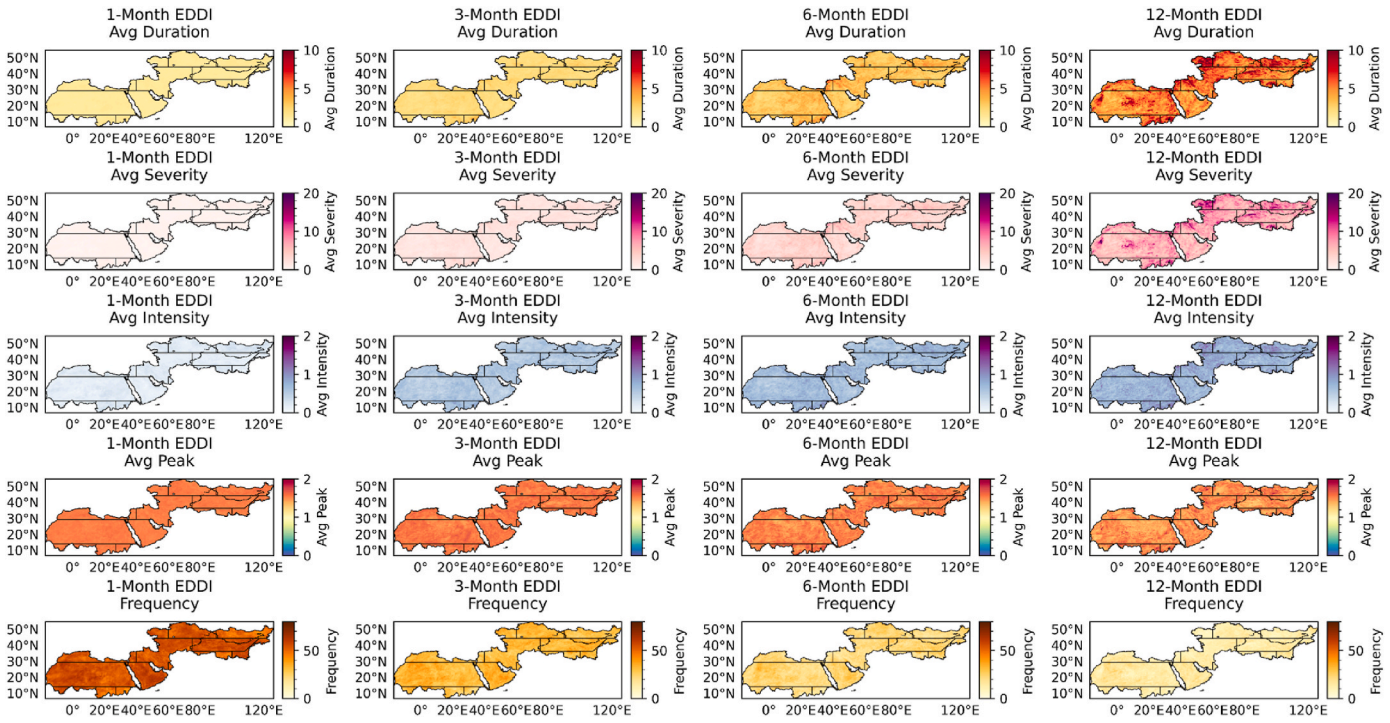

Fig. 8a. Spatial patterns of drought characteristics for 4 different timescales of EDDI during 1983 – 2023: (first-row panels) average drought duration, (second-row panels) average drought severity, (third-row panels) average drought intensity, (fourth-row panels) average drought peak and (fifth-row panels) drought frequency.

with sustained atmospheric demand (Hobbins et al., 2016; Qing et al., 2023). This pattern is evident in the 2010 event (Fig. 11 and Supplementary Fig. S10a–c), where EDDI indicates an earlier onset than SPI by weeks in ARP and SAH. Correlations (Fig. 7 and Table 2) vary regionally: strong negative correlations ($\rho > -0.8$) in WCA, ECA, and WSB indicate balanced precipitation and ET_o influences, while weaker correlations in WSB (-0.40 to -0.72) and TIB (-0.41 to -0.47) reflect limited ET_o--precipitation coupling in complex topography or low-precipitation areas (Vicente-Serrano et al., 2020). Homogeneous inland regions show consistent index agreement, whereas variable margins highlight EDDI differences, with implications for region-specific drought monitoring in arid landscapes.

4.2. Early warning potential and monitoring applications

EDDI provides an early indication of drought onset at short timescales (1–4 weeks), preceding SPI by several weeks, as observed during the 2010 event (Fig. 10). In this case, short-timescale EDDI indicated rapid shifts to severe conditions in ARP and SAH. This early detection stems from EDDI's direct response to anomalies in atmospheric evaporative demand (ET_o), which can signal incipient drying before precipitation deficits accumulate in SPI (McEvoy et al., 2016b). The lead time reflects physical processes, including land–atmosphere coupling, in which an initial high ET_o—driven by factors such as elevated temperature, low humidity, increased radiation, and wind—depletes soil moisture when water is available. This shifts energy partitioning toward sensible heat, warming the near-surface atmosphere and potentially reinforcing high ET_o by reducing latent cooling and lowering boundary-layer humidity. Large-scale circulation anomalies, such as persistent high-pressure systems, can precondition regions by promoting subsidence, clear skies, and adiabatic warming, sustaining elevated ET_o prior to significant precipitation deficits. However, EDDI lead time does not imply causality between ET_o and precipitation reduction, as precipitation deficits may develop independently or through separate atmospheric drivers.

In semi-arid regions with variable precipitation, this early indication allows time for management responses, including irrigation adjustments and early warning for affected sectors, supporting resilience in water-limited systems. The multi-timescale nature of EDDI enables comprehensive drought monitoring: short timescales identify rapid-onset droughts associated with increases in c and rapid declines in soil moisture, while longer timescales (3–12 months) assess impacts on water storage and ecosystems. This capability is relevant for arid regions that experienced increased extremes in ARP and SAH after 2000 (e.g., 2015–2022; Fig. 9), linked to trends in ET_o and temperature (Fig. 5) and to projected changes in atmospheric moisture under warming (IPCC, 2021). The EDDI's multi-timescale capability facilitates comprehensive drought monitoring. At short timescales (e.g., 1–4 weeks), EDDI effectively detects rapid-onset (flash) droughts driven by elevated atmospheric evaporative demand, whereas at longer timescales (3–12 months) it enables assessment of persistent droughts and their impacts on water resources and ecosystems (Hobbins et al., 2016). This versatility supports the integration of EDDI with precipitation-based indices such as SPI and SPEI, enhancing overall drought characterization in arid regions.

4.3. Limitations and uncertainties

Although EDDI demonstrates clear advantages in certain contexts, several limitations require consideration. Its exclusive dependence on ET_o can overestimate drought severity in regions where irrigation or groundwater inputs offset atmospheric demand, decoupling evaporative forcing from actual surface moisture conditions. This issue is relevant in human-modified semi-arid agricultural areas, where land surface responses may differ from those assumed in ET_o calculations. The Penman–Monteith equation used to compute ET_o introduces uncertainties related to input variables, including air temperature, vapor pressure deficit, wind speed, and net radiation. In data-sparse regions, errors in these variables within reanalysis products can propagate and affect trend estimates (Allen et al., 1998; Hobbins et al., 2016). Although the use of consistent reanalysis data (ERA5) reduces some biases, as supported by validations in Asian drylands (Hou et al., 2023), systematic

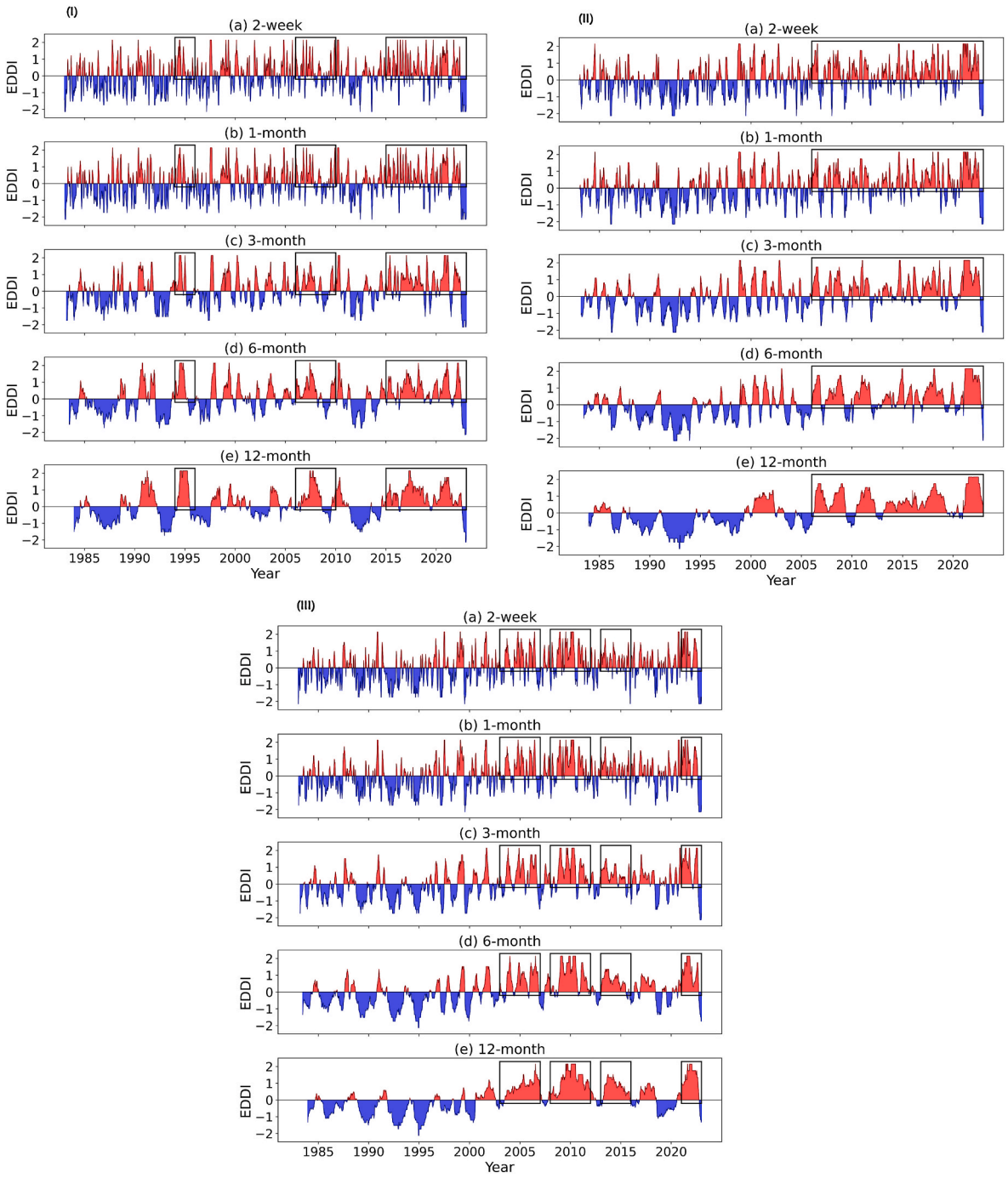

Fig. 9. Time-dependent shifts in EDDI across (a) 2-week, (b) 1-month, (c) 3-month, (d) 6-month, and (d) 12-month periods in some selected regions within the study area from 1983 to 2023, encompassing (I) Arabian Peninsula (ARP), (II) West Central Asia (WCA), and (III) Sahara (SAH). Black rectangles highlight past severe drought occurrences, with red and blue hues indicating dry and wet states.

sensitivity to input errors remains and warrants further analysis. Furthermore, the probabilistic standardization applied in EDDI assumes stationarity in the underlying hydroclimatic distributions. This assumption is increasingly challenged under ongoing climate change, where non-stationary conditions can alter distributional properties and lead to inaccuracies in drought severity classification (Vicente-Serrano et al., 2015). Such effects may contribute to differences between EDDI and precipitation-based indices, such as SPI. Additionally, this study focuses on meteorological drought characterization, and direct linkages to hydrological impacts (e.g., streamflow anomalies), agricultural outcomes (e.g., crop yield reductions), or vegetation responses (e.g., NDVI anomalies) have not been evaluated. Without validation against these impact indicators, inferences about real-world consequences carry uncertainty, and future work should incorporate in situ or remote sensing data to assess drought effects on surface and subsurface processes (Sheffield et al., 2012). Despite these limitations, the consistent spatial and temporal patterns across Figs. 2–11 and Tables 1 and 2 support the utility of EDDI as a complementary tool for drought monitoring in regions dominated by ET_o. Addressing the identified uncertainties through multi-index approaches or adaptive methods could improve monitoring systems. Future studies may benefit from integrating EDDI with additional observational datasets or machine-learning techniques to improve

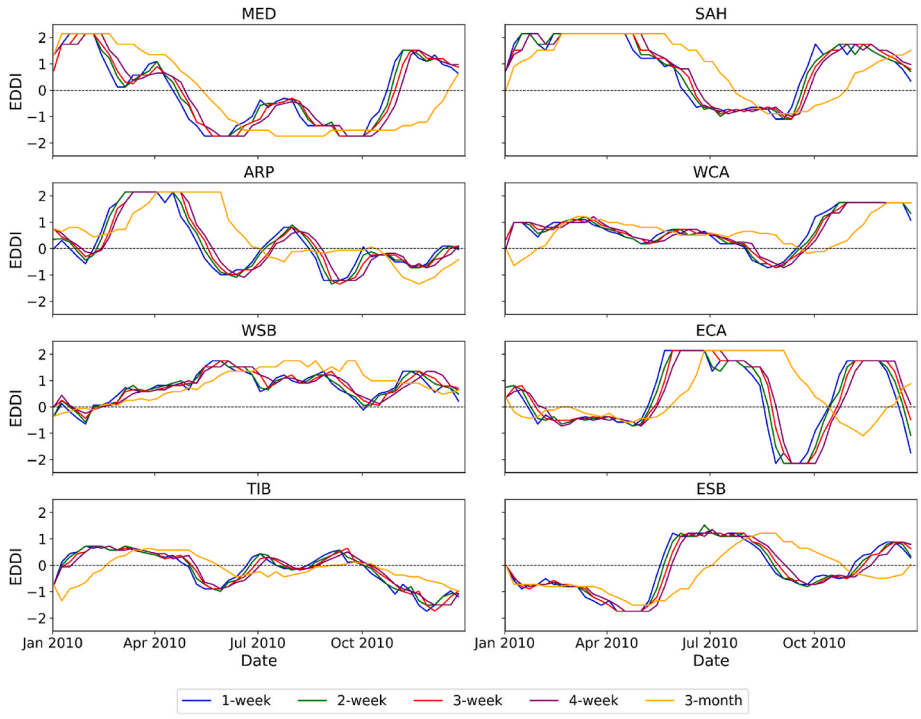

Fig. 10. Time-based changes in EDDI across 1-week to 3-month timescales during the 2010 drought, covering the Mediterranean (MED), Sahara (SAH), Arabian Peninsula (ARP), West Central Asia (WCA), West Siberia (WSB), East Central Asia (ECA), Tibetan Plateau (TIB), and East Siberia (ESB) regions.

drought characterization in arid regions.

5. Conclusion

This study provides a comprehensive evaluation of the EDDI for characterizing drought variability in arid regions of Asia and Africa over the period 1983–2023. Using high-resolution ERA5 reanalysis data and a multi-index comparison with the SPI and SPEI, the analysis addresses gaps in the application of EDDI to arid environments, including its effectiveness in identifying rapid-onset droughts. Key contributions include a spatially detailed comparison of EDDI performance relative to SPI and SPEI across timescales from 1 to 12 months in extensive arid domains, combined with trend detection using the MMK test and Sen's slope estimator. This multi-timescale assessment in underrepresented arid regions enhances the available methods for drought monitoring and early warning.

Statistical results indicate strong negative correlations between EDDI and SPI/SPEI, particularly at shorter timescales, reflecting agreement in drought signaling (positive EDDI values correspond to negative SPI/SPEI values, both indicating drying conditions). For example, in the ARP, correlations reached −0.90 with SPEI and −0.64 with SPI at the 1-month timescale. Spatially, significant drying trends ($p < 0.05$) in EDDI-1 were evident across large portions of the SAH, WCA, ESB, and WSB, associated with increases in ET_o (Sen's slope: 2.0–5.16 mm year^{-1}) and precipitation declines. During the 2010 drought, EDDI demonstrated greater sensitivity to rapid-onset events, detecting deficits 2–4 weeks earlier than SPI in SAH and ARP. Additionally, EDDI identified higher frequencies of moderate-to-extreme drought categories (C2–C4) in Eastern Europe (EEU) compared to SPI, consistent with its response to evaporative anomalies. These results support the use of EDDI as both a complementary and independent index in arid regions. Its formulation, based on ET_o—which incorporates temperature, wind speed, radiation, and humidity—makes it appropriate for environments where atmospheric demand is the primary driver of drought severity. The performance of EDDI at short timescales (1–3 months) corresponds to rapid soil moisture depletion in these areas, providing lead time for management responses.

Increasing drought risks in arid Asia and Africa underscore the need to incorporate indices such as EDDI into operational monitoring systems. Recommended actions include: (1) utilizing reanalysis products like ERA5 to supplement limited in situ observations for high-resolution assessments; (2) integrating EDDI into early warning systems, especially in agriculture-dependent areas such as the Tigris–Euphrates Basin and Sahel, where flash droughts affect substantial rain-fed croplands; and (3) promoting regional cooperation to standardize drought response protocols, as informed by past challenges in basins like the Aral Sea. Implementation of EDDI-based monitoring could inform measures such as water-allocation adjustments and support for drought-resistant practices. Overall, this study confirms the value of EDDI for drought assessment in arid regions under changing climate conditions.

CRediT authorship contribution statement

Akinwale T. Ogunrinde: Writing – review & editing, Writing – original draft, Visualization, Supervision, Software, Methodology, Formal analysis, Data curation, Conceptualization. **Paul Adigun:** Writing – review & editing, Writing – original draft, Validation, Supervision, Methodology, Formal analysis. **Xian Xue:** Writing – review & editing, Supervision, Project administration. **Dairaku Koji:** Writing – review & editing, Supervision, Project administration. **Ermias S. Brhane:** Writing – review & editing.

Declaration of generative AI and AI-assisted technologies in the writing process

During the preparation of this work, the authors used AI-based language models Grok4 and OpenAI GPT-5.1 for text editing and language-related tasks. After using these tools, the authors reviewed and edited the content as needed and take full responsibility for the content of the publication.

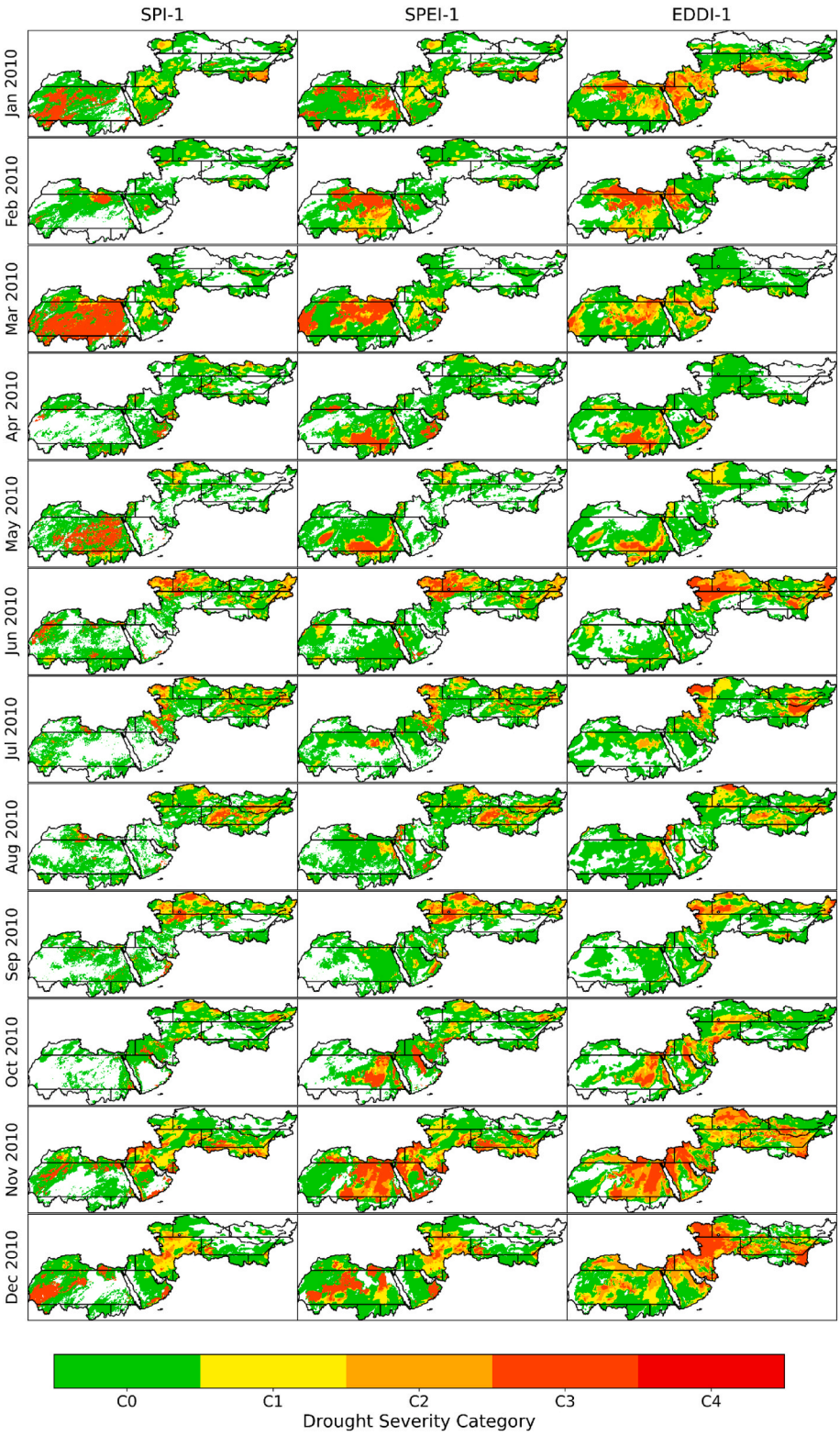

Fig. 11. Spatial and temporal progression of drought severity as shown by EDDI-1, SPI-1, and SPEI-1 throughout the 2010 drought episode.

Funding

The study was supported by Northwest Institute of Ecological Environment and Resources, Chinese Academy of Science (grant number: E429020101).

Declaration of competing interest

The authors declare that they have no known competing financial interests or personal relationships that could have appeared to influence the work reported in this paper.

Acknowledgement

We express our gratitude to the ECMWF team for providing the ERA5 Land reanalysis high-resolution data at no cost, greatly benefiting the academic community and advancing climate research.

Appendix A. Supplementary data

Supplementary data to this article can be found online at https://doi.org/10.1016/j.wace.2026.100873.

Data availability

The data used in this study can be freely downloaded from https://cds.climate.copernicus.eu/datasets/reanalysis-era5-land?tab=download (Hersbach et al., 2020), while the codes will be made available upon reasonable request.

References

Abramowitz, M., Stegun, I.A., 1965. Handbook of Mathematical Functions, with Formulas, Graphs, and Mathematical Tables. Dover Publications, p. 1046. https://personal.math.ubc.ca/~cbm/aands/abramowitz_and_stegun.pdf.

Allen, R.G., Pereira, L.S., Raes, D., Smith, M., 1998. Crop evapotranspiration-Guidelines for computing crop water requirements-FAO irrigation and drainage paper 56. FAO, Rome 300 (9), D05109.

Al-Sakkaf, A.S., Zhang, J., Yao, F., Hamed, M.M., Simbi, C.H., Ahmed, A., Shahid, S., 2024. Assessing exposure to climate extremes over the Arabian Peninsula using ERA5 reanalysis data: spatial distribution and temporal trends. Atmos. Res. 300, 107224. https://doi.org/10.1016/j.atmosres.2024.107224.

Amani, S., Shafizadeh-Moghadam, H., 2023. A review of machine learning models and influential factors for estimating evapotranspiration using remote sensing and ground-based data. Agric. Water Manag. 284, 108324. https://doi.org/10.1016/j.agwat.2023.108324.

ASCE, 2005. The ASCE Standardized Reference Evapotranspiration Equation. The American Society of Civil Engineers, Reston, VA, p. 59. https://ascelibrary.org/doi/abs/10.1061/9780784408056.

Budyko, M.I., 1974. Climate and Life. Academic Press, New York, USA, p. 508.

Christian, J.I., Basara, J.B., Hunt, E.D., Otkin, J.A., Furtado, J.C., Mishra, V., Randall, R. M., 2021. Global distribution, trends, and drivers of flash drought occurrence. Nat. Commun. 12 (1), 6330. https://doi.org/10.1038/s41467-021-26692-z.

Clelland, A.A., Marshall, G.J., Baxter, R., 2024. Evaluating the performance of key ERA-Interim, ERA5 and ERA5-Land climate variables across Siberia. Int. J. Climatol. 44 (7), 2318–2342. https://doi.org/10.1002/joc.8456.

Dai, A., 2013. Increasing drought under global warming in observations and models. Nat. Clim. Change 3 (1), 52–58. https://doi.org/10.1038/nclimate1633.

Donohue, R.J., Roderick, M.L., McVicar, T.R., 2011. Assessing the differences in sensitivities of runoff to changes in climatic conditions across a large basin. J. Hydrol. 406 (3-4), 234–244. https://doi.org/10.1016/j.jhydrol.2011.07.003.

Gebrechorkos, S.H., Sheffield, J., Vicente-Serrano, S.M., Funk, C., Miralles, D.G., Peng, J., Dyer, E., Talib, J., Beck, H.E., Singer, M.B., Dadson, S.J., 2025. Warming accelerates global drought severity. Nature 1–8.

Guha-Sapir, D., Below, R., Hoyois, P., 2021. EM-DAT: the emergency events database. Centre for Research on the Epidemiology of Disasters (CRED). Université catholique de Louvain, Brussels. www.emdat.be. (Accessed 5 March 2025).

Guo, H., Bao, A., Liu, T., Jiapaer, G., Ndayisaba, F., Jiang, L., Kurban, A., De Maeyer, P., 2018. Spatial and temporal characteristics of droughts in central Asia during 1966–2015. Sci. Total Environ. 624, 1523–1538. https://doi.org/10.1016/j.scitotenv.2017.12.120.

Hamed, K.H., Ramachandra Rao, A., 1998. A modified Mann-Kendall trend test for autocorrelated data. J. Hydrol. 204 (1), 182–196. https://doi.org/10.1016/S0022-1694(97)00125-X.

Han, J., Singh, V.P., 2023. A review of widely used drought indices and the challenges of drought assessment under climate change. Environ. Monit. Assess. 195 (12), 1438. https://doi.org/10.1007/s10661-023-12062-3.

Hersbach, H., Bell, B., Berrisford, P., Hirahara, S., Horányi, A., Muñoz-Sabater, J., Nicolas, J., Radu, R., Schepers, D., Simmons, A., Soci, C., Dee, D., Thépaut, J.N., 2020. The ERA5 global reanalysis. Q. J. R. Meteorol. Soc. 146 (730), 1999–2049. https://doi.org/10.1002/qj.3803.

Hobbins, M.T., Wood, A., McEvoy, D.J., Huntington, J.L., Morton, C., Anderson, M., Hain, C., 2016. The evaporative demand drought index. Part I: linking drought evolution to variations in evaporative demand. J. Hydrometeorol. 17 (6), 1745–1761. https://doi.org/10.1175/JHM-D-15-0088.1.

Hou, C., Huang, D., Xu, H., Xu, Z., 2023. Evaluation of ERA5 reanalysis over the deserts in northern China. Theor. Appl. Climatol. 151 (1), 801–816. https://doi.org/10.1007/s00704-022-04306-y.

Immerzeel, W.W., Lutz, A.F., Andrade, M., Bahl, A., Biemans, H., Bolch, T., Hyde, S., Brumby, S., Davies, B.J., Elmore, A.C., Emmer, A., Feng, M., Fernández, A., Haritashya, U., Kargel, J.S., Koppes, M., Kraaijenbrink, P.D.A., Kulkarni, A.V., Mayewski, P.A., Nepal, S., Pacheco, P., Painter, T.H., Pellicciotti, F., Rajaram, H., Rupper, S., Sinisalo, A., Shrestha, A.B., Viviroli, D., Wada, Y., Xiao, C., Yao, T., Baillie, J.E.M., 2020. Importance and vulnerability of the world's water towers. Nature 577 (7790), 364–369. https://doi.org/10.1038/s41586-019-1822-y.

IPCC, 2021. Summary for policymakers. In: Masson-Delmotte, V., et al. (Eds.), Climate Change 2021: the Physical Science Basis. Contribution of Working Group I to the Sixth Assessment Report of the Intergovernmental Panel on Climate Change. Cambridge University Press, Cambridge, United Kingdom and New York, NY, USA, pp. 3–32. https://www.ipcc.ch/report/ar6/wg1. (Accessed 5 March 2025).

Kapoor, D., Bhardwaj, S., Landi, M., Sharma, A., Ramakrishnan, M., Sharma, A., 2020. The impact of drought in plant metabolism: how to exploit tolerance mechanisms to increase crop production. Appl. Sci. 10 (16), 5692. https://doi.org/10.3390/app10165692.

Kumar, V., Sharma, K.V., Pham, Q.B., Srivastava, A.K., Bogireddy, C., Yadav, S.M., 2024. Advancements in drought using remote sensing: assessing progress, overcoming challenges, and exploring future opportunities. Theor. Appl. Climatol. 155 (6), 4251–4288. https://doi.org/10.1007/s00704-024-04914-w.

Lovino, M.A., Pierrestegui, M.J., Müller, O.V., Müller, G.V., Berbery, E.H., 2024. The prevalent life cycle of agricultural flash droughts. npj Clim. Atmos. Sci. 7 (1), 73. https://doi.org/10.1038/s41612-024-00618-0.

McEvoy, D.J., Huntington, J.L., Mejia, J.F., Hobbins, M.T., 2016a. Improved seasonal drought forecasts using reference evapotranspiration anomalies. Geophys. Res. Lett. 43 (1), 377–385. https://doi.org/10.1002/2015GL067009.

McEvoy, D.J., Huntington, J.L., Hobbins, M.T., Wood, A., Morton, C., Anderson, M., Hain, C., 2016b. The evaporative demand drought index. Part II: CONUS-wide assessment against common drought indicators. J. Hydrometeorol. 17 (6), 1763–1779. https://doi.org/10.1175/JHM-D-15-0122.1.

McKee, T.B., Doesken, N.J., Kleist, J., 1993. The relationship of drought frequency and duration to time scales. In: Proceedings of the 8th Conference on Applied Climatology. American Meteorological Society, Boston, MA, pp. 179–183. https://www.droughtmanagement.info/literature/AMS_Relationship_Drought_Frequency_Duration_Time_Scales_1993.pdf.

Mishra, A.K., Singh, V.P., 2010. A review of drought concepts. J. Hydrol. 391 (1), 202–216. https://doi.org/10.1016/j.jhydrol.2010.07.012.

Naumann, G., Alfieri, L., Wyser, K., Mentaschi, L., Betts, R.A., Carrao, H., Spinoni, J., Vogt, J., Feyen, L., 2018. Global changes in drought conditions under different levels of warming. Geophys. Res. Lett. 45 (7), 3285–3296. https://doi.org/10.1002/2017GL076521.

Ng, C.Y., Wan Jaafar, W.Z., Othman, F., Lai, S.H., Mei, Y., Juneng, L., 2024. Assessment of evaporative demand drought index for drought analysis in Peninsular Malaysia. Sci. Total Environ. 917, 170249. https://doi.org/10.1016/j.scitotenv.2024.170249.

Ogunrinde, A.T., Xian, X., Adigun, P., Adawa, I.S., Zhao, D., Xing, Z., Temitope, I.J., 2024a. Assessing teleconnection influences on the spatial and temporal patterns of meteorological drought in Northwest China. Big Earth Data 8 (4), 703–731. https://doi.org/10.1080/20964471.2024.2392448.

Ogunrinde, A.T., Adeyeri, O.E., Xian, X., Yu, H., Jing, Q., Faloye, O.T., 2024b. Long-term spatiotemporal trends in precipitation, temperature, and evapotranspiration across arid Asia and Africa. Water 16 (22), 3161. https://doi.org/10.3390/w16223161.

Ogunrinde, A.T., Adigun, P., Xian, X., Yu, H., Koji, D., Adebiyi, A., Sabo, A.A., 2024c. Multi-scale drought variability over West Africa and the associated large-scale circulation patterns. Geomat. Nat. Hazards Risk 15 (1), 2409199. https://doi.org/10.1080/19475705.2024.2409199.

Ogunrinde, A.T., Adigun, P., Xue, X., Dairaku, K., Shah, S.A., Adawa, I.S., 2025. Probabilistic quantification of global drought risk amplification from temperature-enhanced evapotranspiration under climate change. Geosci. Front. 102235.

Qing, Y., Wang, S., Yang, Z.L., Gentine, P., Zhang, B., Alexander, J., 2023. Accelerated soil drying linked to increasing evaporative demand in wet regions. npj Clim. Atmos. Sci. 6 (1), 205.

Safdar, M., Shahid, M.A., Zaman, M., Rasul, F., Muzammal, H., Raza, A., Sabir, R.M., Zafar, U., 2023. Drought monitoring with multiple indices and management through various techniques: a review. Eng. Proc. 56 (1), 307. https://doi.org/10.3390/ASEC2023-16602.

Sharafi, S., Ghaleni, M.M., 2023. Enhancing drought monitoring and prediction in diverse climates by using composite drought indices. Stoch. Environ. Res. Risk Assess. 1–21. https://doi.org/10.1007/s00477-023-02597-9.

Shawaqfeh, S., Al Tawaha, A.R.M., Gunal, H., Al-Tawaha, A.R., Qotb, M.A., Karnwal, A., Rashid, R., 2025. Climate change and drought: challenges for agriculture in arid environments. In: Sustainable Agriculture Under Drought Stress. Academic Press, pp. 3–13. https://doi.org/10.1016/B978-0-443-23956-4.00001-6.

Sheffield, J., Wood, E.F., Roderick, M.L., 2012. Little change in global drought over the past 60 years. Nature 491 (7424), 435–438. https://doi.org/10.1038/nature11575.

Tanarhte, M., De Vries, A.J., Zittis, G., Chfadi, T., 2024. Severe droughts in North Africa: a review of drivers, impacts and management. Earth Sci. Rev. 250, 104701. https://doi.org/10.1016/j.earscirev.2024.104701.

UNCCD, 2022. Drought in Numbers 2022: Restoration for Readiness and Resilience. United Nations Convention to Combat Desertification, Bonn.

UNCCD, 2024. Three-quarters of Earth's land became permanently drier in last three decades. Unit. Nation Conven. Combat Desertif. https://www.unccd.int/news-stories/press-releases/three-quarters-earths-land-became-permanently-drier-last-three-decades.

Van Loon, A.F., 2015. Hydrological drought explained. Wiley Interdiscip. Rev. Water 2 (4), 359–392. https://doi.org/10.1002/wat2.1085.

Vicente-Serrano, S.M., Beguería, S., López-Moreno, J.I., 2010. A multiscalar drought index sensitive to global warming: the standardized precipitation evapotranspiration index. J. Clim. 23 (7), 1696–1718. https://doi.org/10.1175/2009JCLI2909.1.

Vicente-Serrano, S.M., Van der Schrier, G., Beguería, S., Azorin-Molina, C., Lopez-Moreno, J.I., 2015. Contribution of precipitation and reference evapotranspiration to

drought indices under different climates. J. Hydrol. 526, 42–54. https://doi.org/10.1016/j.jhydrol.2014.11.025.
Vicente-Serrano, S.M., Quiring, S.M., Peña-Gallardo, M., Yuan, S., Domínguez-Castro, F., 2020. A review of environmental droughts: increased risk under global warming? Earth Sci. Rev. 201, 102953.
Wang, H., Pan, Y., Chen, Y., 2017. Comparison of three drought indices and their evolutionary characteristics in the arid region of northwestern China. Atmos. Sci. Lett. 18 (3), 132–139.
Wild, M., 2009. Global dimming and brightening: a review. J. Geophys. Res. Atmos. 114 (D10), D00D16. https://doi.org/10.1029/2008JD011470.
Wilks, D.S., 2011. Statistical Methods in the Atmospheric Sciences, vol.100. Academic Press.
Wu, D., Chen, J., Xiong, L., Lee, J.H., Kim, J.S., Moon, H.T., 2024. Assessing global drought conditions under climate change: a comparison of stationary and non-stationary approaches and identification of hotspot regions. J. Hydrol. 640, 131663. https://doi.org/10.1016/j.jhydrol.2024.131663.
Yevjevich, V., 1967. An Objective Approach to Definitions and Investigations of Continental Hydrological Droughts (Hydrology Papers 23). Colorado State University, Fort Collins, Colorado.
Zhang, L., Jiao, W., Zhang, H., Huang, C., Tong, Q., 2017. Studying drought phenomena in the Continental United States in 2011 and 2012 using various drought indices. Rem. Sens. Environ. 190, 96–106. https://doi.org/10.1016/j.rse.2016.12.010.